Raja Ramanna
Centre for Advanced Technology Indore

Annual Progress Report :2015-16

Raja Ramanna Centre for Advanced Technology, Indore

Annual Progress Report :2015-16

Sr. No.	Contents	Page No.
I.	Indus Synchrotrons	2
II.	Accelerator Technology	10
III.	Laser Technology	19
IV.	Laser Applications	24
V.	Materials Science	34
VI.	International Collaboration	36
VII.	Infrastructure	37
VIII.	Human Resource Development	39
IX.	Outreach Activities	39

I. INDUS SYNCHROTRONS

A. Indus accelerators: operation

Both the synchrotron radiation sources, Indus-1 and Indus-2, were operated round-the-clock. Indus-2 was operated at beam current up to 200 mA and 2.5 GeV energy while Indus-1 was operated at 100 mA current and 450 MeV energy. The Indus-2 storage ring is operating with a highly stable electron beam. For example, the high frequency perturbations have been brought down to 3 microns (rms) in the horizontal plane and 2 microns (rms) in the vertical plane. The user orbit in Indus-2 was optimized to a new orbit with minimized closed orbit distortion, which eliminated the need for applying orbit bumps for individual beam lines and the beam life time improved from 15 hours to 18 hours at 100 mA at 2.5 GeV. The temperatures of the dipole chambers during machine operation also came down within safe limits, thus facilitating Indus-2 operation for the users at higher stored beam currents. The improved performance of the Indus synchrotron radiation sources is reflected in a substantial increase in the number of users. The user experiments have more than doubled from 190 in 2013 to 390 in 2015. During 2015 the availability of 13 beamlines in Indus-2 for user experiments was ~ 4370 hours.

B. Upgradation of Indus -2

1. Commissioning of permanent magnet plane polarized undulators U1 and U2

The two planar undulators U1 and U2, one for Atomic, Molecular and Optical Science (AMOS) beamline and another for Angle Resolved Photoelectron Spectroscopy (ARPES) beamline, installed last year in the Indus-2 storage ring, were commissioned. At 2.5 GeV beam energy, the effect of operation of undulators on the beam optics was studied by changing pole gap of the undulators from 250 mm (maximum) to 25 mm (minimum) in several steps. The changes in closed orbit distortion (COD) were measured on all 56 beam position indicators (BPIs) distributed all over the ring. The maximum changes in the COD were 0.12 mm in horizontal plane and 0.055 mm in vertical plane when the magnet pole gap of both the undulators were kept at 25 mm, confirming the placement of the undulators in the Indus-2 storage ring with the required accuracy. Both the undulators U1 and U2 were first commissioned at a low stored beam current of ~ 4 mA. After successful commissioning, the current was upgraded in steps to a current > 100 mA in November 2015. The main challenge for operating the undulator with higher stored beam current was handling its highly intense SR beam. For the safety of vacuum chamber, the interlock limits based on beam position were determined experimentally by defining an allowable close orbit movement detected at

the insertion device beam position indicators. At 2.5 GeV with beam current ~108mA, an exercise of step-by-step gradual pole gap variation of U1 undulator was started from its initial maximum value of 250 mm up to minimum value of 25 mm. During these trials, the maximum closed orbit distortion deviations were controlled below 20 microns in both horizontal and vertical planes; there was no significant change in betatron tune values, the temperature of vacuum chamber, vacuum and beam lifetime. Images of the synchrotron radiation beam emitted from the undulator and its neighboring bending magnet were recorded using a fluorescent screen beam viewer. The beam images from U1 are shown in Fig. 1. It can be seen that the synchrotron radiation emitted from the undulator is much brighter than that from the bending magnet.

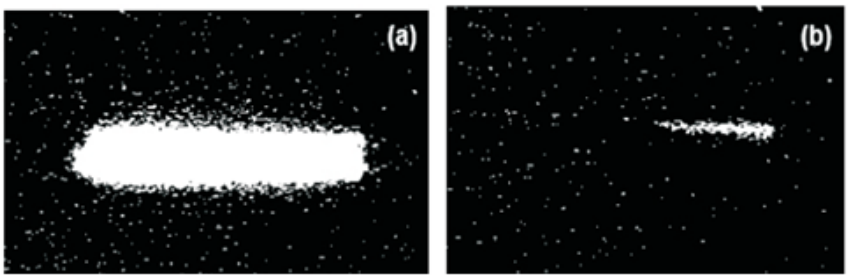

Fig. 1: Beam image of the synchrotron radiation beam emitted (a) from the undulator U1 for pole gap of 25 mm and (b) from the neighboring bending magnet when the U1 pole gap is at its maximum value of 250 mm.

2. Installation of APPLE-2 undulator

An APPLE-2 (Advanced Planar Polarized Light Emitter-2) type undulator made of permanent magnet blocks was installed in the long straight section, LS-5, of Indus-2, after carrying out offline tests. The undulator consists of four standard Halbach-type permanent magnet rows where two rows situated above and two rows below the plane of the electron orbit. Two diagonally opposite rows are coupled and allowed to translate along the axis with respect to the other two diagonally opposite fixed rows in order to change the state of the polarization of synchrotron radiation. This insertion device will be used for generating radiation with adjustable polarization and to enhance the peak spectral brightness of synchrotron radiation by two to three orders of magnitude in the spectral region from 300 eV to 2000 eV including higher harmonics. For installation of the undulator several ultra high vacuum compatible peripherals for the undulator like tapered vacuum chamber and beam position indicator assemblies were designed and manufactured by precision machining and TIG welding. The off-line tests of the APPLE-2 undulator included movement of the poles after connecting the system to the control rack, using the local touch panel testing of remote control functionality and interlocks of the device, beam dynamical studies and analysis of the measured magnetic field data of the undulator. These offline tests were followed by precise placement of the undulator weighing 7.2 MT at the designated location in Indus-2 satisfactorily, under various

constraints from the machine. Precision survey measurements were done before opening of the ring to record the present working positions of the position-sensitive components in the designated section, and then the undulator was installed within +/- 0.1 mm accuracy in the section.

The undulator vacuum chamber coated with non-evaporable getter (NEG) was installed inside the pole gap of undulator in its position using the support stand. This was connected with the peripheral components like taper chambers, insertion device beam position indicators (IDBPI) and bellows. The assembly is isolated with two RF sector valves from the rest of the Indus-2 ring. This undulator vacuum segment was leak-tested and baked followed by NEG coating activation and the ultimate vacuum of 1.4 x 10^{-10} mbar was achieved. Fig. 2 shows the undulator assembly after installation in the Indus-2 storage ring.

Fig. 2: APPLE-2 undulator installed in LS-5 along with the compatible vacuum chamber and other peripherals.

3. Upgradation of control electronics for Indus-2 and booster synchrotron

The control systems of Indus accelerators, microtron injector and industrial accelerators have been upgraded and new sub systems have been added. These include undulator control system for remote and safe operation of undulators from control room, upgradation of Indus-2 data logging system at a higher rep-rate of 1 Hz. Further, a beam based alignment system has been installed in Indus-2 to minimise the closed orbit distortion of its orbit, higher beam life time, reduced variation in machine tune and reduced corrector strength. A control system (hardware and software) for beam based alignment was developed to control 72 active shunt power supplies. Prototype processing electronics using an embedded web server for monitoring the beam position monitors of the booster synchrotron at a higher repetition rate of 1 kHz was developed.

4. Design, development and installation of upgraded stripline kicker magnets and upgradation of low conductivity water system

Stripline kickers are an integral part of the bunch-by-bunch feedback system and are devices fed with RF power for providing transverse correction kick to the electron beam in an accelerator. With a view to enhance the performance of the bunch-by-bunch feedback system and hence improved beam stability, design, development and installation of upgraded versions of ultra high vacuum compatible horizontal and vertical stripline kickers has been carried out. Fig. 3 shows the inside view of both magnets.

The Indus-2 low conductivity water (LCW) plant is used for cooling of accelerator components, power devices in magnets and RF power supplies etc. and is operated round-the clock. The system was upgraded to increase the process cooling water temperature stability to better than ±0.7^{o}C as compared to the earlier stability of ±1^{o}C. This has helped in improving the stability of Indus-2 operation.

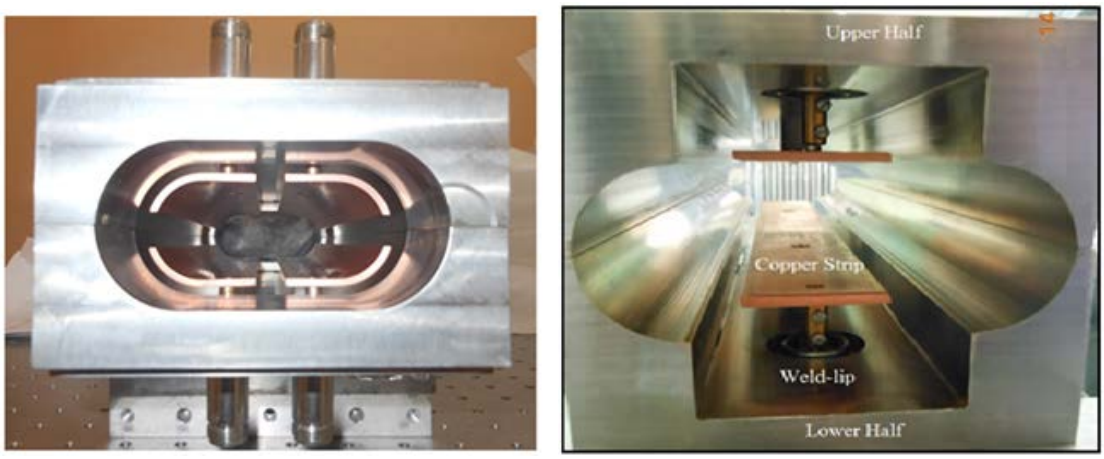

Fig. 3: The inside view of the assembled horizontal and vertical stripline kicker magnets

5. Development of a new microtron for Indus SRS facilities

A new, improved 20MeV injector microtron has been developed (Fig. 4) for Indus synchrotron radiation source facility of RRCAT. The beam was accelerated up to 22nd orbit where the beam energy is 20 MeV. A beam current of 30 mA was measured in the 22nd orbit (Fig. 5)

Fig. 4: Inside view of the new microtron

Fig. 5: Beam current waveform in the 22nd orbit (beam extraction orbit) of the new microtron at beam energy of 20 MeV. The beam current is shown in pink trace (scale each division = 10 mA).

6. **Upgradation of various magnet power supplies in the Indus synchrotron source facility**

The magnet power supplies used in Indus-1 and Indus-2 have been upgraded. These include four power supplies (80 A, 25 V) for quadrupole magnets in the transport line TL-2 which feeds the electron beam from the booster synchrotron to Indus-1 and three in the transport line TL-3 which feeds the electron beam to Indus-2. The new power supplies feature a modular design, better thermal management, simpler configuration, smaller filtering requirements and better layout for easy maintenance. Further, four numbers of fast orbit feedback (FOFB) power supplies and three numbers of active shunt power supplies for independent adjustment of Indus-2 quadrupole currents were also developed.

High voltage DC and pulsed power supplies have also been developed for ECIL for use in an explosive detection system.

C. Indus beamlines commissioning, up-gradation and utilization

The Indus synchrotron radiation sources, a national facility, are being used by scientists and students from various universities, national institutes and research laboratories all over the country. A soft x-ray reflectivity beamline (BL-3) has been commissioned recently, which is the 13th beamline on Indus-2 and operates in the energy range of 100 eV to 1500 eV. This beamline is based on a constant deviation angle variable line spacing plane grating monochromator. It can be very useful for resonant x-ray reflectivity measurements of a large number of low Z elements and 3d

transition metal thin films for the determination of structural and interfacial characteristics and also for the measurement of reflectivity of mirrors, efficiency of gratings and detectors, transmission of thin film filters and multilayers. Test experiments have been carried out successfully, and the beamline is now open to users. Fig. 6 shows the picture of the experimental station of this beamline.

Some of the operating beamlines have been equipped with advanced user facilities. A closed cycle cryostat (CCR) based cooling system (shown in Fig. 7) and a high temperature stage have been installed in the image plate of the angle dispersive x-ray diffraction (ADXRD) beamline (BL-12). A new high temperature stage (upto 1100 K) has been commissioned which can be used both in the scanning extended x-ray absorption fine structure (EXAFS) beamline (BL-9) as well as the dispersive EXAFS beamline (BL-8). A Fourier transform infrared (FTIR) system with a closed cycle cryostat has been installed at the photo-physics beamline at Indus-1 (BL-5). A dedicated beamline is under fabrication for the utilization of the light emitted from the newly installed APPLE-2 undulator. The most important application of circular polarized light is in the study of magnetic materials by carrying out x-ray magnetic circular dichroism (XMCD) experiments.

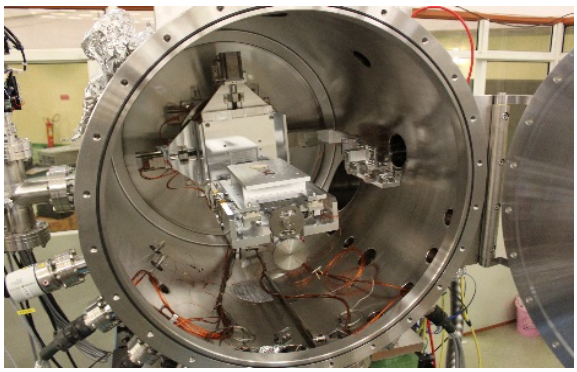

Fig. 6: Two-axis high-vacuum compatible goniometer with x-y-z sample manipulation stage of the soft x-ray reflectivity beamline (BL-3).

Fig. 7: The closed cycle cryostat based sample cooling stage installed at the image plate of the angle dispersive x-ray diffraction (ADXRD) beamline (BL-12).

Using the x-ray lithography beamline (BL-7) of Indus-2, x-ray lenses for use in the hard x-ray regime have been fabricated in a new antimony free material, code named SUEX. Fig. 8 shows the scanning image micro-graph (SEM) of the lenses. A focal beam diameter with full width at half maximum (FWHM) of 0.8 micron (Fig. 9) was obtained when this lens was used at the Diamond Light Source, UK. Next, Fresnel zone plates (FZP) with a focal length of 25 mm have been fabricated in polymethyl methacrylate (PMMA) on ultra-thin titanium film using 30 keV electron-

beam lithography. These have been designed for focusing of capillary discharge based argon x-ray laser (wavelength: 46.9 nm).

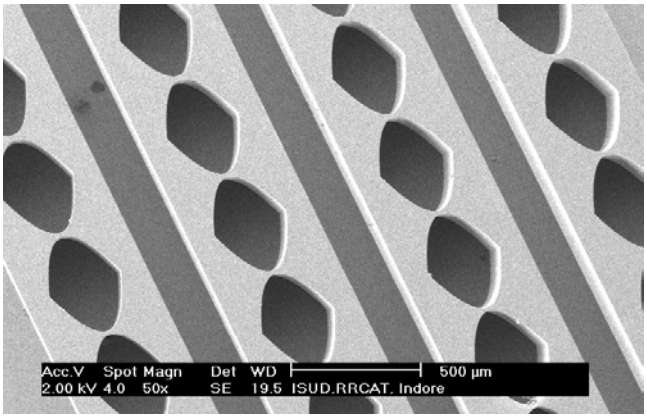

Fig. 8: Scanning electron microscope image of the SUEX lenses developed at BL-7 beamline.

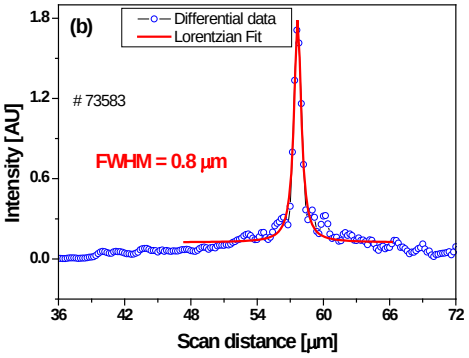

Fig. 9: Beam profile of the x-ray beam at the focus of the x-ray lens.

During 2015, the Indus beamlines have been widely utilized by users for a variety of experiments. Some examples are studies of oxygen absorption edge in $Ni_xZn_{1-x}O$ at the soft x-ray absorption beamline (BL-1), imaging studies on tristructural-isotropic (TRISO) nuclear fuel micro-pellets at the imaging beamline (BL-4), development of long period fibre grating using x-ray lithography beamline (BL-7), x-ray absorption studies on complex formation for the trapping of Eu^{3+} ions by cucurbit(n)uril molecules at the extended x-ray absorption fine structure (EXAFS) beamline (BL-9), high pressure x-ray diffraction (XRD) measurements using the extreme condition energy dispersive/angel dispersive (ED/AD) XRD beamline (BL-11) for identifying the various phase transitions with pressure in $NaZr_2(PO_4)_3$ system, studies on the structure of Co_3TeO_6 for understanding its complex magnetic properties at ADXRD beamline (BL-12), characterizing gold nanoparticles on silicon substrate using x-ray standing waves at the x-ray fluorescence (XRF) beamline (BL-16) and determination of new protein structures at the protein crystallography beamline (BL-21). Figures 10 and 11 show some results from the EXAFS beamline and the protein crystallography beamline respectively.

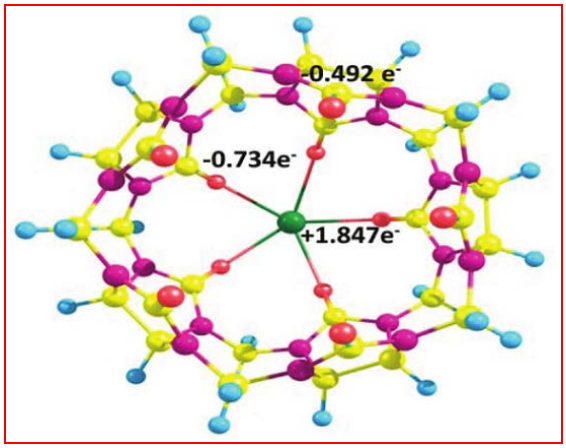

Fig. 10: Optimised structure of the complex of Eu^{3+} ion (green circle) with the molecule of Cucurbit(5)uril determined using the EXAFS beamline (BL-9).

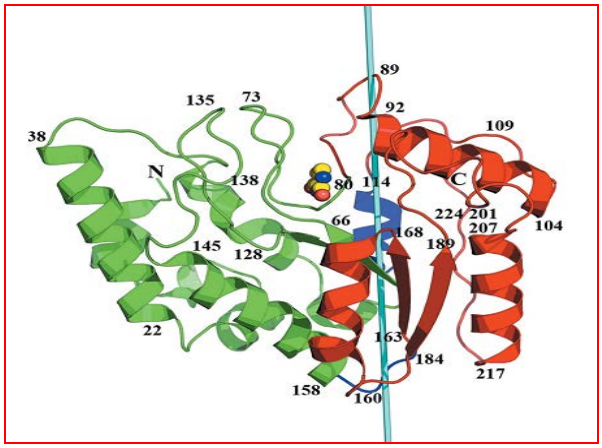

Fig. 11: Structure of uracil-DNA glycosylase from Mycobacterium tuberculosis determined at the protein crystallography beamline (BL-21).

Work on the installation and vacuum testing of various components for beamlines and front ends has also been carried out. The front end for the Indus-2 photo emission electron microscope (PEEM) beamline (BL-22) has been designed, fabricated and commissioned (Fig .12). Some of the components like pre-masks, water cooled beam viewer, scanning wire monitors etc. have been designed, indigenously fabricated and installed in the front ends of insertion devices based atomic, molecular and optical studies (AMOS) and angle resolved photo-electron spectroscopy (ARPES) beamlines (Fig.13). A compact two stage differential pumping system (length 415 mm) has been developed, tested and installed on the BL-3 of Indus-2 to provide a windowless transition between high and low vacuum regions of the beamline.

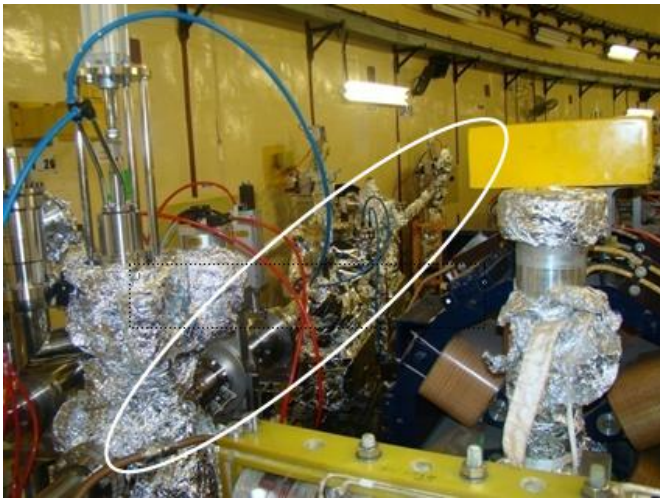

Fig 12: View of the photo emission electron microscope (PEEM) beamline (BL-22) front end that has been installed on the Indus-2 ring.

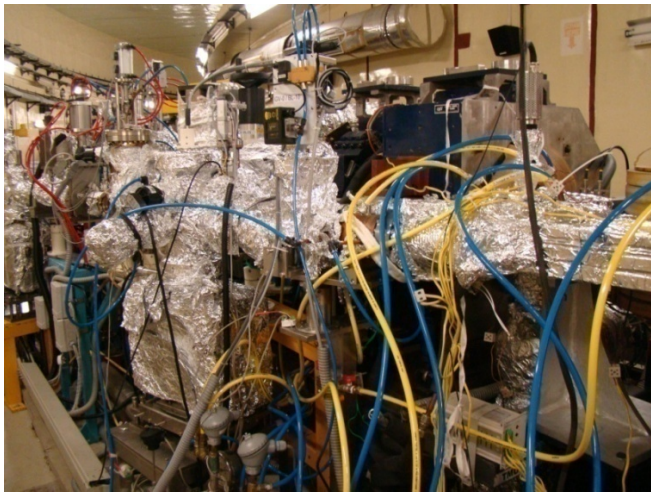

Fig 13. View of the front end components in BL-10 (Angle resolved photoelectron spectroscopy beamline).

II. ACCELERATOR TECHNOLOGY

1. Polishing of nine-cell 1.3 GHz superconducting radio-frequency cavity

A facility for processing of multi-cell 1.3 GHz superconducting radio-frequency (SCRF) cavities has been set up at RRCAT. Using this facility a nine-cell 1.3 GHz SCRF cavity (Fig. 14) has been fabricated and is undergoing processing using in-house developed facilities. The cavity was inspected on an indigenously developed optical inspection bench. No major defects were observed during the inspection of the cavity. Thickness of the cavity was measured at 136 locations using an ultrasonic thickness gauge. Processing of the cavity is being carried out using a standard recipe followed at international lab, which includes 120 micron electropolishing (bulk polishing), high temperature annealing at 600° C for 10 hours, 25 micron electropolishing (light polishing), ultrasonic rinsing, high pressure rinsing, assembly of RF couplers and vacuum leak testing in class-100 clean-room, low temperature baking at 120° C for 48 hours and RF test at 2 K in vertical test stand facility. As a first step, the cavity has been electro-polished to remove an average of 50 micron material from equator region and high pressure rinsed using ultra-pure water at 120 bar. The cavity is now ready for the second stage polishing and will be tested at 2 K for required performance in terms of quality factor and accelerating gradient.

Fig. 14: Electro-polishing of the nine-cell 1.3 GHz superconducting radio-frequency cavity.

2. Indigenous development of semi-automatic cavity tuning machine

A semi-automatic cavity tuning machine (Fig. 15) has been designed and developed for the RF resonating frequency and field flatness correction of a multi-cell 1.3 GHz superconducting radio-frequency (SCRF) cavity. The tuning machine has motor driven tuning jaws, cavity mounting system and bead pull measurement system. A tuning methodology to tune a multi-cell cavity has been developed and trials have been carried out on a nine-cell 1.3 GHz cavity.

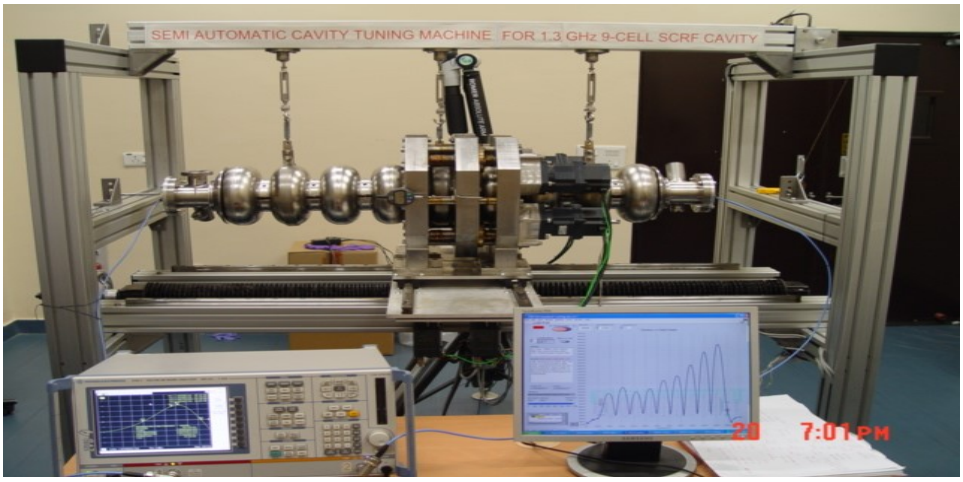

Fig. 15: A nine-cell 1.3 GHz SCRF cavity on semi-automatic tuning machine.

3. Indigenous development of a centrifugal barrel polishing machine

A centrifugal barrel polishing machine (Fig. 16) has been indigenously designed and developed for polishing of the internal surface of multi-cell superconducting radio-frequency (SCRF) cavities. The machine has a provision to simultaneously polish 4 numbers of five-cell 650 MHz SCRF cavities in four barrels.

Fig. 16: Centrifugal barrel polishing machine loaded with single-cell 650 MHz cavity.

4. Fabrication of 650 MHz SCRF cavity by indigenously developed laser welding technique

RRCAT had developed an innovative laser welding technique for fabrication of superconducting radio-frequency (SCRF) cavities. A 1.3 GHz test cavity was welded using this technique and had demonstrated performance matching international standards. A Japanese patent was granted for this procedure. This technique has been used now to fabricate a single-cell 650 MHz SCRF cavity (Fig. 17) which is much larger in size. Development of multi-cell cavities at 650 MHz is essential for building a high intensity pulse proton linac which will be used in the long term Indian spallation neutron source (ISNS) programme.

Fig. 17: The 650 MHz laser-welded superconducting radio-frequency cavity.

5. Enhancement of liquefaction capacity of indigenous helium liquefier

Helium liquefaction using a completely indigenous system was first achieved at RRCAT in 2010. The system was based on reciprocating type expansion engine and used cross counter flow type heat exchangers. This system has now been upgraded with the development of new reciprocating type cryogenic expansion engines with larger refrigeration capacity and state of the art brazed aluminum plate fin heat exchangers with high heat transfer rate and efficiency. High efficiency brazed aluminum plate fin heat exchangers manufactured in the country have been successfully deployed in a helium liquefaction system for the first time. The upgraded system produces more than 35 litres of liquid helium per hour (Fig. 18).

Fig 18: Indigenously developed helium liquefier of 35 litre/hr capacity.

6. Design of horizontal test cryostat

A horizontal test cryostat has been designed under the Indian Institutions-Fermilab collaboration (IIFC) for testing two 650 MHz “dressed” superconducting radio-frequency (SCRF) cavities at 2K in a single testing cycle. This cryostat will be the third such system in the world and will be used to test 5-cell 650 MHz SCRF cavities in CW / pulsed regime being developed at RRCAT. The design has been reviewed and approved by international experts. Fig. 19 shows the finalized 3-D model of the horizontal test cryostat.

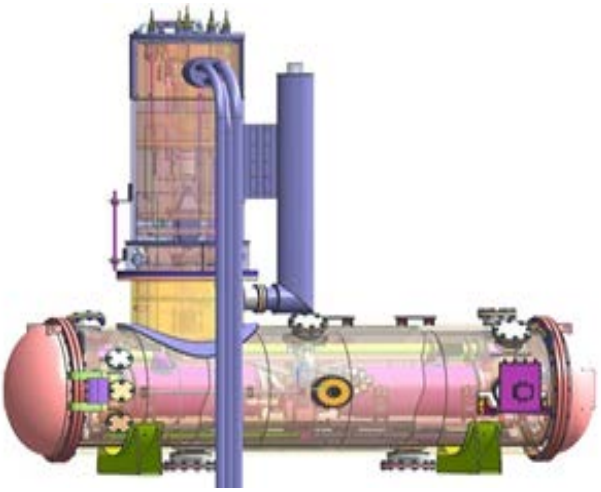

Fig 19: 3-D model of the horizontal test cryostat.

7. Indigenous development of RF cavity and high power coupler for Indus-2

A bell-shaped tuneable oxygen-free copper radio-frequency (RF) cavity and high power input coupler operating at 505.8 MHz for Indus-2 has been indigenously designed, fabricated and tested (Fig. 20). The RF cavity half shells, ports and cooling tubes are joined using precision fixtures by four stage vacuum brazing process. To keep higher order modes (HOM) within safe limits, extensive water cooling is provided on the cavity body, ports and coupler parts to get a temperature stability within ± 0.1°C. The cavity achieved an ultimate vacuum of $5x10^{-10}$ mbar after baking and cool down. . High power testing of RF cavity was carried up to 33 kW net average RF power meeting the consistent operational requirements of Indus-2. During the entire testing no significant multipacting, arcing or oscillations were observed.

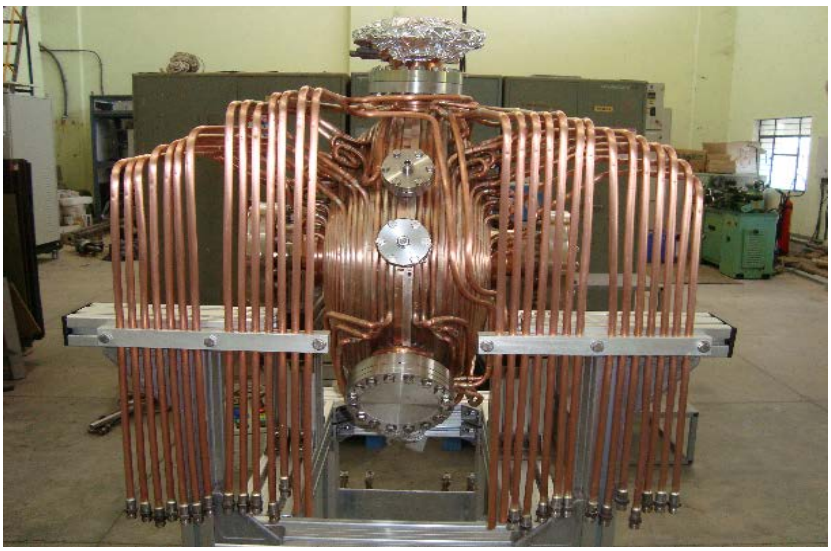

Fig. 20: High purity copper radio-frequency cavity at 505.8 MHz with copper cooling coils.

8. Development and deployment of digital low-level radio-frequency (DLLRF) control system in all four RF stations of Indus-2

All four radio-frequency (RF) stations of Indus-2 have been now upgraded with field programmable gate array (FPGA) based digital low level RF (LLRF) control system (Fig. 21). After replacing the analogue LLRF systems with digital LLRF systems, feedback control parameters were optimized in all four stations to achieve phase stability of better than 0.5° and amplitude stability of better than 0.5%. Also feedback loop bandwidth was optimized for all four stations to accumulate the beam at injection energy and successfully ramping the energy to achieve stored beam of more than 200 mA at 2.5 GeV. Development of the DLLRF system involves use of latest technologies of digital signal processing, RF signal processing and fast feedback control systems.

Fig. 21: Digital LLRF systems installed with four RF stations in Indus-2.

9. Magnet technology

All the different types of magnets required in the Indus synchrotron sources have been developed in-house. In a continuing effort to further improve the performance, prototype harmonic sextupole magnets (Fig. 22) and low coupling impedance kicker magnets (Fig. 23) for Indus-2 have been developed. Harmonic sextupole magnets are required to suppress the non-linearity induced by the existing chromatic sextupole magnets and thereby to improve the dynamic aperture in Indus-2 storage ring. A prototype magnet with low carbon steel core has been developed and characterized for integrated magnetic field strength and quality. The overall physical length is kept within 250 mm to accommodate it in the existing available space in the beam direction of Indus-2. Infrastructure for magnet testing has been augmented by development of pulsed type MH loop tracer system for characterization of high energy permanent magnets and a stretched wire system for the measurement of magnetic field integrals of planar undulators. A spin wave measurement set up has been developed to measure power handling capability of ferrites and garnets for development of high power (100 kW) CW ferrite circulators at RRCAT.

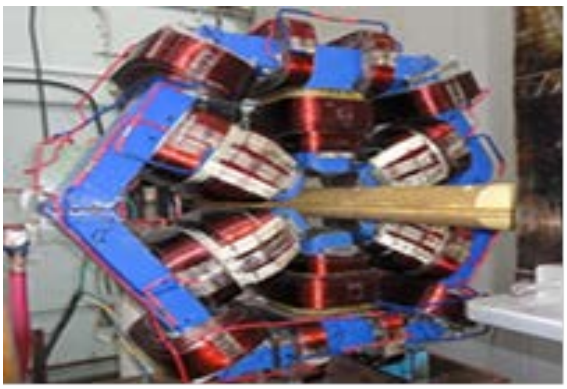

Fig. 22: Prototype harmonic sextupole magnet for Indus-2.

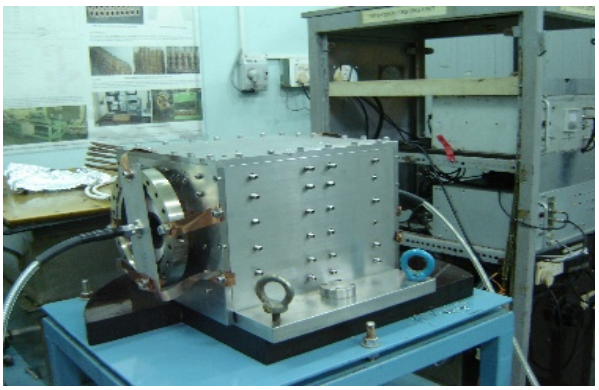

Fig. 23: Low coupling impedance kicker magnet for Indus-2.

10. Developments in linac technology

A 10 MeV electron linac suitable for operation under industrial conditions has been developed with mostly indigenous design and component manufacturing. Its supervisory control system facilitates remote operation of the linac from a control room and ensures personnel safety, fail safe and reliable operation. At present, the developed linac (Fig. 24) has delivered a beam power of 4.2 kW and has been tested for a continuous running of more than 90 hours.

Fig. 24: The 10 MeV industrial linac. The linear accelerating structure, focusing magnetic elements and the beam scanner can be seen.

11. Infra-red free electron laser (IRFEL) development

Development of an infra-red free electron laser (IR-FEL) designed to lase in a wavelength range as 15 – 50 μm using a 15 – 25 MeV electron beam from an injector linac and a 2.5 m long pure permanent magnet undulator with 50 mm period has been completed. This FEL employs an indigenously developed injector linac system with employing a 476 MHz sub-harmonic pre-buncher and two S-band two plane wave transformer (PWT) linac structures developed in-house (Fig. 25). The main challenge in this PWT linac assembly was precision machining followed by precision brazing to ensure UHV leak tightness and precision spacing of the copper disks. A low level S-Band LLRF system has been designed and developed for phase and amplitude stabilization of microwave power to be fed to injector linac of IRFEL. The electron beam transport line magnets and the vacuum beam line for the IR-FEL have been built in-house, tested off-line and installed in the IR-FEL setup. Design vacuum has been achieved in the complete vacuum beam line. A vacuum system has been designed, fabricated and tested for the 14 meter, variable cross-section beam transport line. The system is able to maintain the required vacuum level of better than 3×10^{-8} mbar throughout the line. Commissioning and testing of individual sub-systems of the IR-FEL is presently in an advanced stage (Fig. 26).

Fig. 25: The plane wave transformer linac for the infra-red free electron laser.

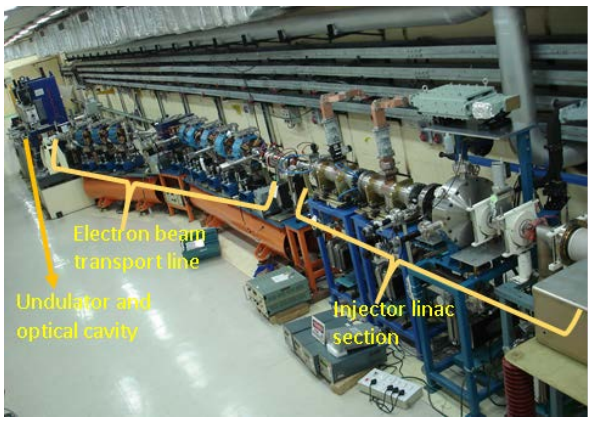

Fig. 26: The 60 m long shielded tunnel showing the free electron laser being assembled in place.

12. Installation and commissioning of a ultraclean controlled atmosphere brazing furnace

An indigenously built hydrocarbon-free ultraclean cold walled controlled atmosphere brazing furnace has been installed (Fig. 27) to facilitate brazing of dissimilar metal transition joints and copper-to-copper joints for accelerator components. The furnace has demonstrated a fast pump down time of less than an hour, an ultimate vacuum of 5×10^{-7} mbar and a temperature uniformity of ± 5°C. It can also operate in dynamic argon partial pressure of 0.5 mbar. Apart from fulfilling the brazing requirements of various accelerator projects, this ultraclean furnace environment has also facilitated development of new brazing recipes for joining of niobium and copper to austenitic stainless steels.

Fig, 27. The controlled atmosphere brazing furnace

13. Development of components for the Indian spallation neutron source (ISNS) programme

The physics design of low energy beam transport (LEBT) line and medium energy beam transport (MEBT) line for the injector linac has been completed. The LEBT matches and transports

the beam from the ion source to the entrance of radio-frequency quadrupole (RFQ), MEBT matches and transports the beam from the exit of RFQ to the entrance of single spoke resonator (SSR). The electromagnetic design and beam dynamics studies have been completed for three families of single spoke resonators to accelerate the beam in three different ranges of beam energy.

A multicusp type H^- ion source has been developed for high current H^- injector linac (Fig. 28). The developed multicusp filament based H^- ion source has been operated up to 50 keV energy with extraction of 6 mA H^- ion current, in pulsed mode with 0.5 ms pulse duration and 2 Hz repetition rate.

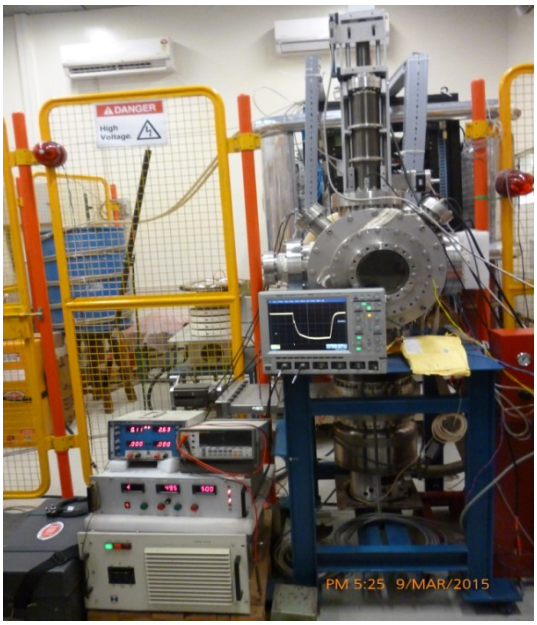

Fig. 28: Filament based multicusp H^- ion source

A prototype high purity alumina ceramic chamber with titanium end flanges was designed and developed (Fig. 29). Such chambers with a thin metallic coating are required for injection kickers magnets in order to avoid shielding of a fast-changing kicker field, minimize eddy current heating, and to carry beam-induced image current.

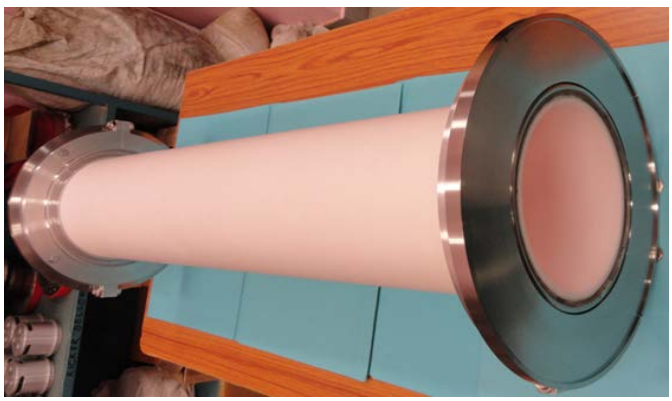

Fig. 29: Alumina ceramic chamber with titanium end flanges for injection kicker magnets.

III. LASER TECHNOLOGY

1. Development of 20 kW peak power Nd:YAG laser for welding of niobium superconducting radio-frequency cavities

A fiber coupled pulsed Nd:YAG laser providing pulses of 20 kW peak power has been developed (Fig. 30) specifically for laser welding of up to 4 mm thick niobium superconducting radio-frequency (SCRF) cavities. The pulse duration can be varied from 2 to 60 ms and pulse repetition rate from 1 to 100 Hz. This laser system has been equipped with two time shared fiber optic ports of 600 micron core diameter, one for full depth welding of niobium SCRF cavities and another for surface smoothening to achieve good quality weld joint with minimum heat affected zone, distortions and shrinkage. The laser delivers an average power of 1 kW.

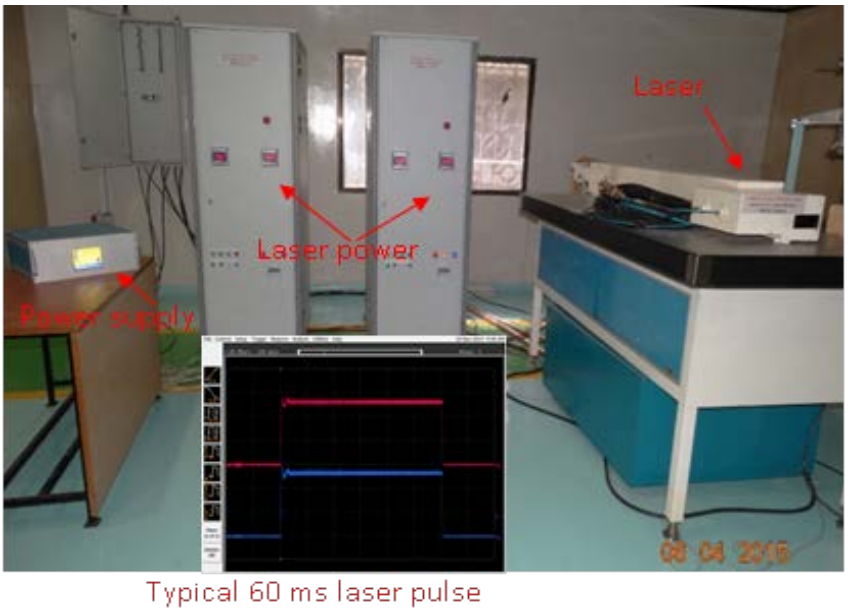

Fig. 30: The 20 kW peak power Nd:YAG laser for welding of superconducting radio-frequency cavities.

2. Development of a pulsed Nd:YAG laser for remote dismantling of irradiated fuel subassemblies of the prototype fast breeder reactor (PFBR)

A pulsed Nd:YAG laser of a 10 kW peak power average power with dual port fiber optic beam delivery (Fig. 31) has been developed for remote dismantling of irradiated fuel subassemblies of the prototype fast breeder reactor (PFBR) in hot cell at IGCAR. It provides pulses with duration variable in the range of 2 to 40 ms and repetition rate in the range of 1 to 100 Hz. Laser system parameters has been optimized for cutting of hexagonal fuel subassemblies of 3 mm thickness in the presence of slippery and pyrophoric sodium at a radiation level of about 106 rad/hr.

Fig. 31: 10 kW peak power fiber coupled pulsed Nd:YAG laser for IGCAR.

3. Development of lasers for material processing applications

An Yb-doped CW fiber laser of 400 W output power (Fig. 32) has been developed using a single oscillator. The all-fiber integration involved minimization of splice joint loss of various fiber components, fiber coupled pump diodes and recoating of these joints to reduce losses. This has led to a high optical-to-optical conversion efficiency of 71%. Laser output is emitted from a 20 micron core diameter of Yb-doped fiber with a nearly-gaussian beam profile (M^2 ~ 1.04). A diode side-pumped continuous wave (CW) Nd:YAG laser of output power 1 kW operating at 1060 nm wavelength has also been developed (Fig. 33). The laser has a double pump head resonator and each pump head is made to accommodate 27 diodes of 80 W power each. The output is coupled to a fiber of 400 micron diameter. Both these lasers are useful for material processing applications.

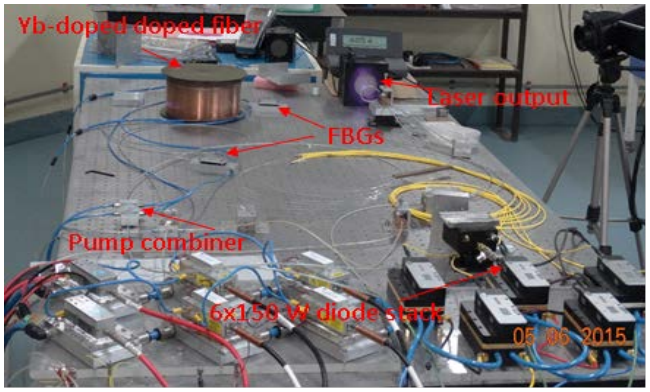

Fig. 32: 400 W all-fiber Yb-doped CW fiber laser.

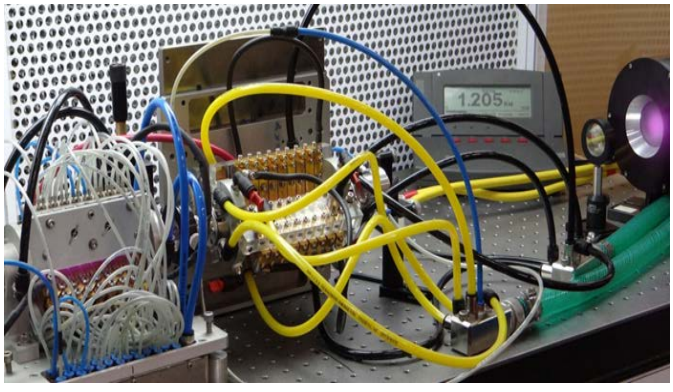

Fig. 33: 1 kW CW Nd:YAG laser.

4. Development of 25 W Erbium-doped fiber laser in eye-safe region

An Er-doped fiber laser emitting at the eye-safe wavelength of 1600 nm has been developed (Fig. 34). It uses a large mode-area Er-doped fiber pumped by a 976 nm diode laser and has a CW output power of 25 W. Due to large quantum defect of ~ 39% between the pump and lasing wavelengths, a water cooled heat sink for the fiber had to be designed to enable laser operation at such a high output power.

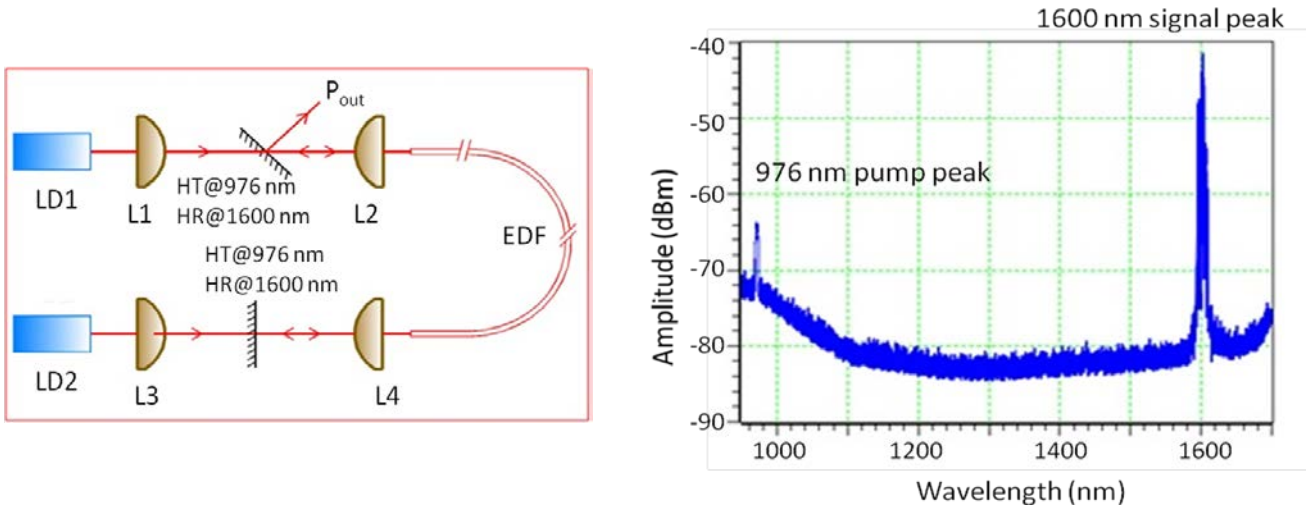

Fig. 34: (a) A schematic view of 25 W Er-doped CW fiber laser and (b) laser output spectrum with peak at 1600 nm.

5. Development of engineered model of diode-pumped solid state green laser

A user-friendly engineered version of diode-pumped solid-state green laser operating at 532 nm has been developed (Fig. 35). The laser delivers ~ 40W of average power at 6.25 kHz repetition rate with less than 40 ns of pulse duration, and has control and safety features suitable for remote operation. The laser was continuously operated for 15 hours and output power, pulse timing jitter and pointing beam stability of the green beam was measured and found to be satisfactory. Two such engineered models of DPSS green lasers have been delivered to BARC and successfully installed there.

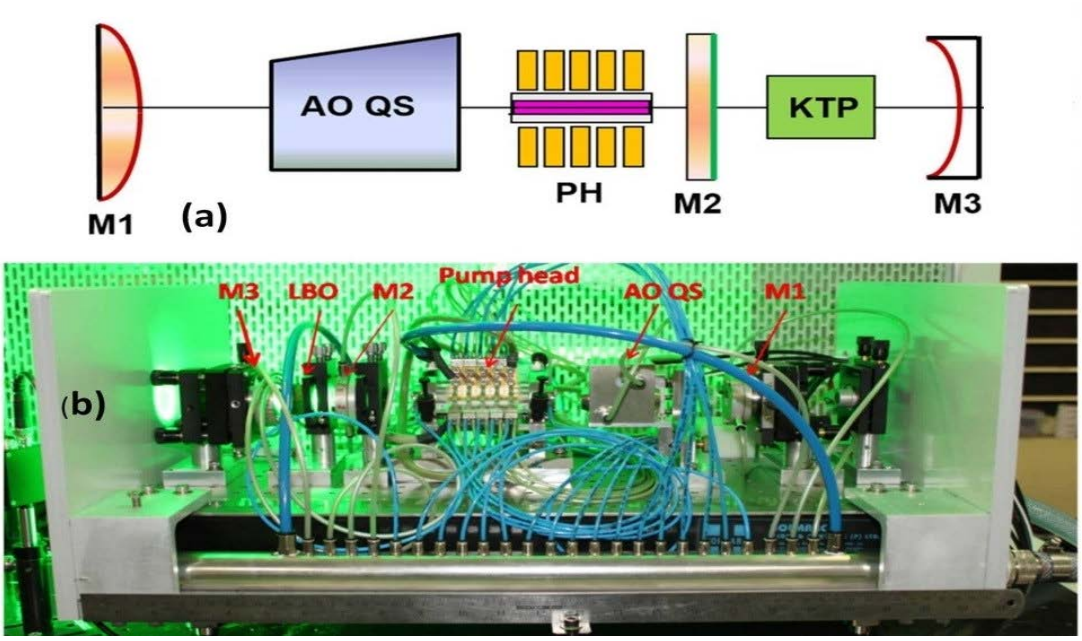

Fig. 35: (a) Schematic of the diode-pumped solid-state green laser, (b) internal layout of the engineered model.

6. Development of wide aperture xenon chloride (XeCl) excimer laser

A wide aperture (30 mm inter-electrode separation) XeCl excimer laser at λ= 308 nm capable has been developed (Fig. 36). The laser cavity has been designed for high pointing stability and high tolerance for misalignment (~ 50 mrad). The laser is suitable for material processing applications.

Fig. 36: Wide aperture xenon chloride excimer laser

7. Testing and quality control of indigenously developed laser glass

Testing and quality control parameters and procedures have been evolved for the Nd-doped phosphate laser glass indigenously developed in collaboration with CGCRI, Kolkata (Fig. 37).

Performance of such glass rods has been studied by using them in the high power laser chain at RRCAT and the quality is found to be of international standards. The quality control of the laser glass rods has been done by measuring several spectroscopic and physical properties of the laser glass like refractive index, non-linear refractive index, Abbe number, stimulated emission cross section, fluorescence peak, fluorescence lifetime, and attenuation coefficient at 1053 nm and 3000 cm^{-1}. These quality control procedures will allow us to study batch by batch production performance of the laser glass fabrication process technology in future.

Fig. 37: A typical Nd:glass slab and a 40 mm diameter, 310 mm long Nd:glass rod made from a similar slab.

8. Development of Fizeau interferometer for optical testing of large size Nd-Phosphate laser amplifier discs.

A large beam diameter (250 mm) Fizeau interferometer has been developed (Fig. 38) for surface quality testing of polished large laser amplifier discs. Liquid paraffin is used as the optical reference flat surface. This interferometer was successfully tested for surface flatness of a 200 mm diameter polished optical window with a flatness of λ/6 at 633 nm.

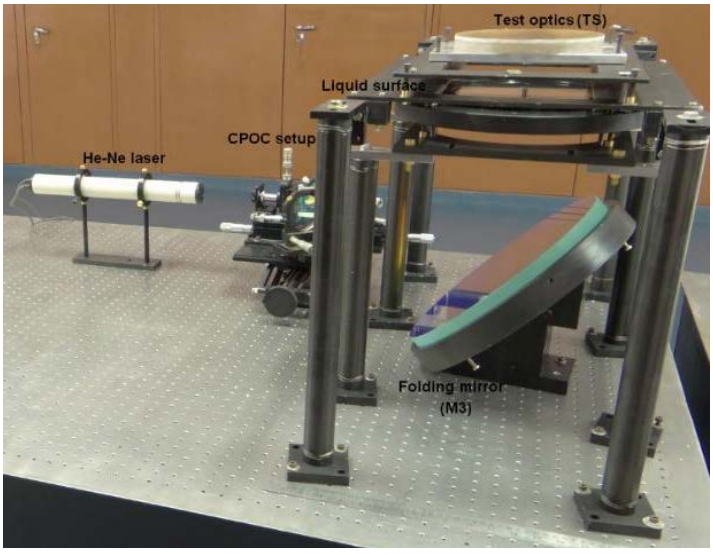

Fig. 38: Part of the Fizeau interferometer developed for testing of large diameter optics.

9. Development of semiconductor lasers and detectors

Photonic devices based on GaAs and InP semiconductors have been fabricated. These include laser diode arrays operating at 980nm with 23.5 W peak power under pulsed operation and 3 W CW power (Fig. 39), GaAs based radiation hard (100 kGy for gamma rays) quadrant detectors operating in the wavelength range of 200-900 nm (Fig. 40) and a novel gold/semiconductor hybrid detector that can simultaneously measure the degree of circular polarization and intensity of a laser beam.

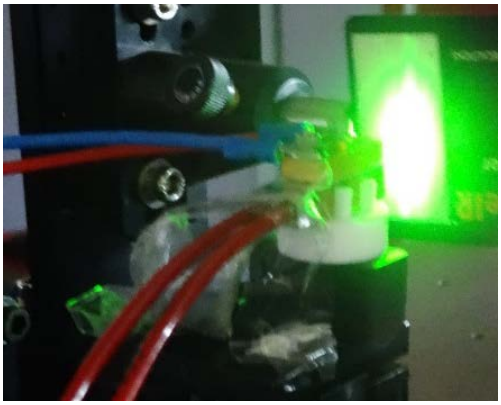

Fig. 39: The diode array laser and its output on a fluorescent screen.

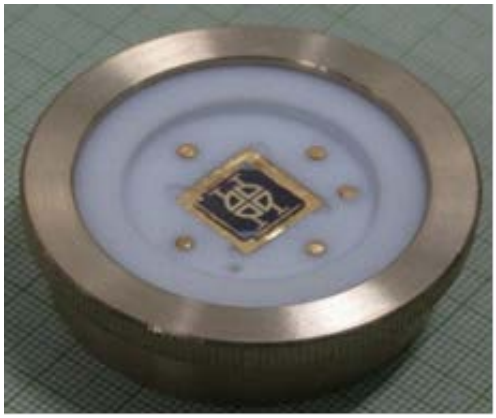

Fig. 40: Radiation hard GaAs based quadrant detector.

IV. LASER APPLICATIONS

1. Development of laser cutting tool and technique for axial and circular cutting of steam generator (SG) tubes for Kaiga generating station-4 reactor

In some of the nuclear power reactors such as that at Kaiga generating station -4 (KGS-4) there is a problem of over rolling of steam generator (SG) tubes in tube sheet. In such cases the removal of leaky SG tubes by mechanical pull out requires very high load strength. A laser based axial grooving technique has been developed for Kaiga Generating Station -4 reactor to reduce the pull out strength of over-rolled steam generator (SG) tubes to a value below 2 ton for tubes which earlier required 5 ton of pull out strength (Fig. 41). This procedure has been qualified at KGS-4 and will be deployed for removal of leaky SG tubes during the next biennial shutdown of KGS-4.

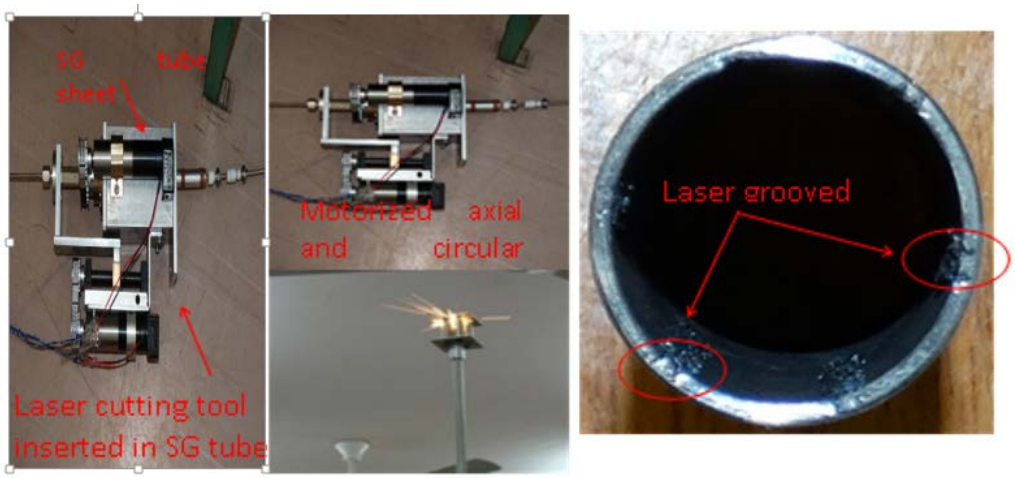

Fig. 41: Laser cutting mock up, fixture for laser cutting of steam generator (SG) tube and laser grooved sample of SG tube.

2. Water-jet assisted underwater laser cutting of damaged and flared fuel assemblies of Dhruva reactor

An in-house developed remotely operated water-jet assisted underwater laser cutting technology was deployed for cutting of damaged portion of 12 numbers of highly radioactive spent fuel assemblies (Fig. 42). The aluminum fuel assemblies (2.5 mm thick and ~ 4 m length) were stored at the bottom of a 5 m deep water column at the spent fuel storage bay of the Dhruva reactor complex. Using the laser cutting technique these were salvaged successfully for reprocessing without any airborne activity and with a very small radiation dose of ~600 mR.

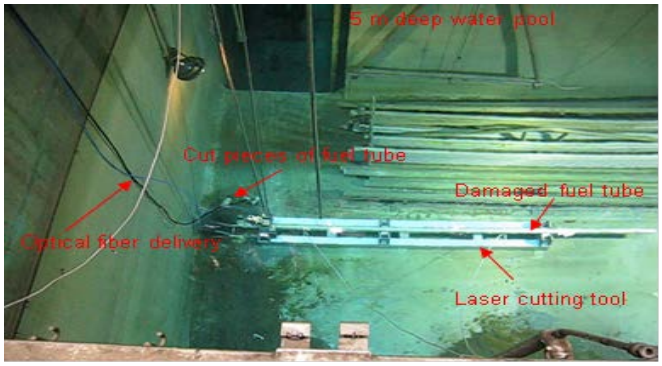

Fig. 42: A view of water-jet assisted underwater laser cutting of damaged fuel tubes in spent fuel storage bay of Dhruva reactor complex.

3. SG tube cutting at Kudankulam nuclear power plant

At the Kudankulam Nuclear Power Project (KKNPP) Unit-2 micro-cracks were suspected in some of the steam generator tubes and it was required to cut three steam generator tubes for radiography and hydro tests. An Nd:YAG laser with flexible fiber optic beam delivery and miniature cutting nozzle was developed and deployed for cutting of ~300 mm length of three steam generator

tubes at SG-2 location of the Kudankulam power plant reactor KKNPP-2 for leak analysis purposes and future reference (Fig. 43). This job was not possible by mechanical methods due to space constraints.

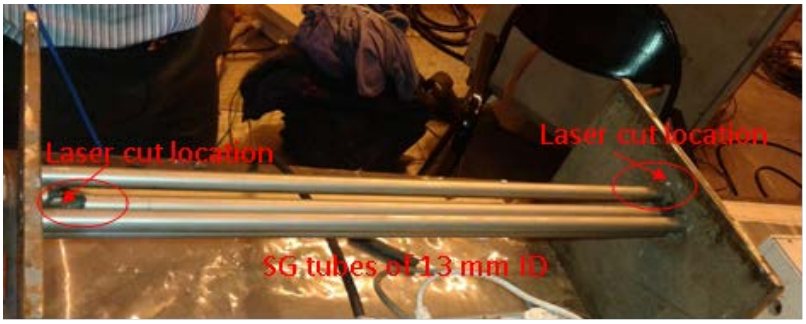

Fig. 43: A view of laser cut location of steam generator tube during mock-up trials at KKNPP-2.

4. In-situ laser cutting of Q-16 coolant channel from KAPS-2 reactor

Heavy water (D_2O) leak was detected from Q-16 coolant channel of KAPS-2 reactor after 20 years of commercial operation due to a fine crack near rolled joint portion of pressure tube. It was required to remove it from reactor core so that the reactor could be put back in operation and also for post-irradiation examination (PIE) of pressure tube. This coolant channel was successfully removed using a custom designed laser cutting system (Fig. 44), which was not possible by mechanical methods due to space restrictions.

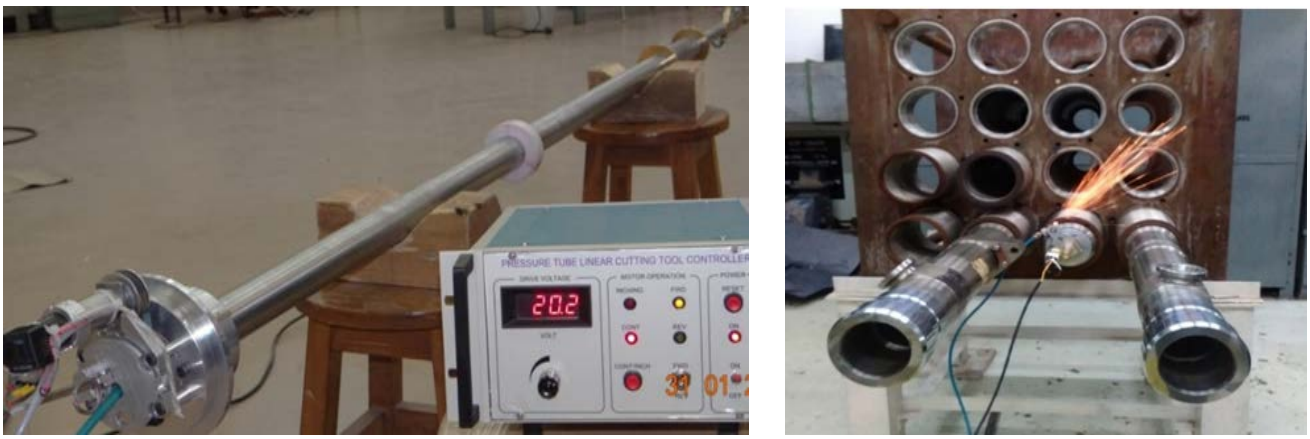

Fig. 44: (a) A view of underwater laser cutting tool for pressure tube stubs, and (b) laser cutting mock-up of bellow lip after cutting of outboard end-fitting.

5. Novel thin foil target for quasi-mono-energetic ion acceleration

Quasi-mono-energetic acceleration of ions has been demonstrated at RRCAT from the interaction of intense, ultra-short laser pulses with specially designed targets. The targets consist a

few nanometers thick coating of gold followed by a top coating of few tens of nanometer thick carbon layer, on an aluminium (Al), silicon or Mylar substrate surface. A 150 TW Ti:sapphire laser beam is focused on the target to a peak intensity of 3 x 10^{19} W-cm^{-2} . The hydrodynamic expansion of gold layer is inhibited due to the presence of the carbon layer. As a result, all the gold ion of different charged species created by the plasma get confined to a narrow energy range. Computer simulations for the above target geometry also corroborate the experimental results. Fig. 45a shows Thomson parabola tracks of heavy gold ions Au ions with different charge states but the same energy (Fig. 45b).

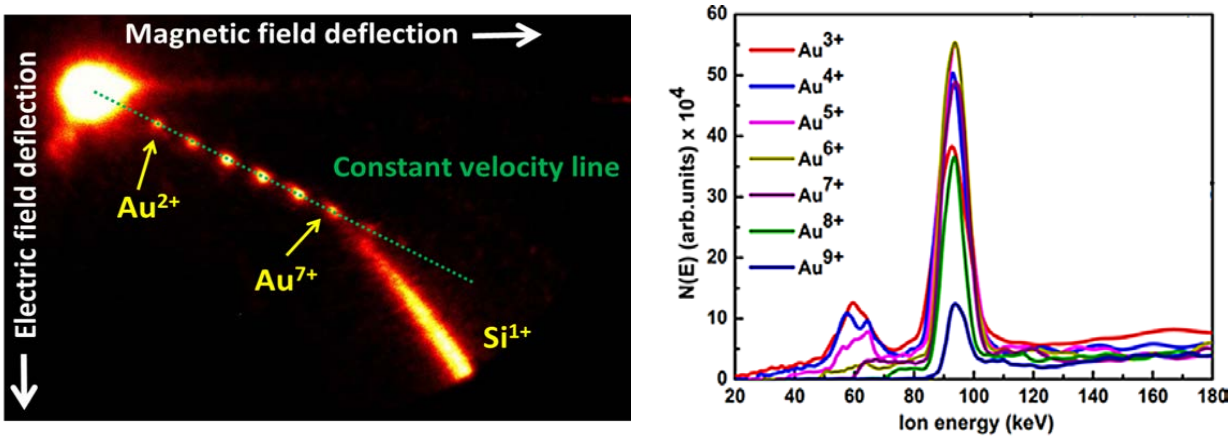

Fig. 45: (a) Thomson parabola trace showing different charge states of gold (Au) ions, (b) the energy spectrum of different charge states.

6. Collimated MeV fast electron beam at grazing incidence laser - solid interaction

A collimated beam of fast electrons has been generated by laser-solid interaction at grazing incidence. The divergence (FWHM) of the electron beam was measured to be 9.8º and 5.3º in the horizontal and vertical directions, respectively (Fig. 46). The energy of the electron beam was in the range 300 keV to 1 MeV.

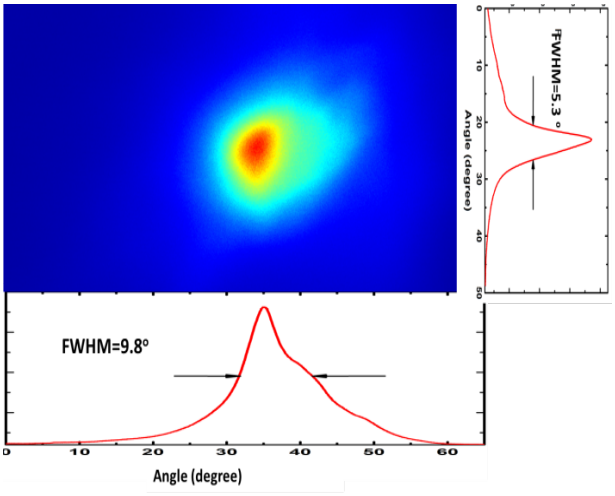

Fig. 46: A typical spatial profile of the hot electron beam.

7. Oblique laser peening technique for tubular SS304L to improve stress corrosion cracking resistance

A laser shock peening technique was developed to inhibit stress corrosion cracking (Fig. 47). Results on tubular SS304L components showed that the surface area affected by stress corrosion cracking reduced from 25% to less than 2% after peening.

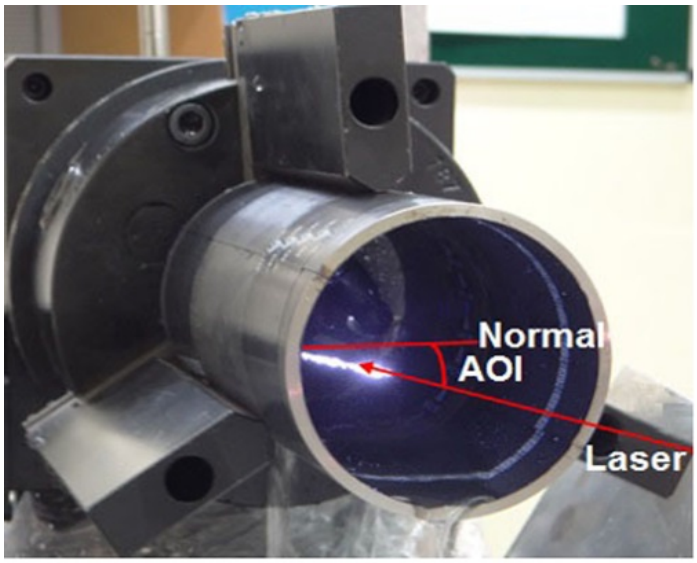

Fig. 47: Oblique laser peening set up

8. Cone-shell Raman spectroscopy for depth-sensitive measurements in layered tissue

A Raman spectroscopic system based on the technique of cone-shell Raman spectroscopy (CSRS) was developed for non-contact, depth-sensitive measurement of layered biological tissue (Fig. 48). The system uses a 785 nm diode laser and three identical axicons for Raman excitation of the target sample in the form of a hollow conic section. Apart from its ability of probing larger depths (~ few mm), a noteworthy feature of the system is that the probing depths can be varied by simply varying the separation between axicons in the excitation arm. Further, no adjustment is required in the sample arm, which is a significant advantage for non-contact, depth-sensitive measurement. The performance of the CSRS system was evaluated by measuring the depth-sensitive Raman spectra from a layered non-biological phantom made of paraffin and acetaminophen and also from a chicken tibia with muscle tissue (thickness ~2.5 mm) on its top. The results demonstrated the ability of the CSRS system to recover Raman spectra of layers located at depths of ~ 2-3 mm beneath the surface.

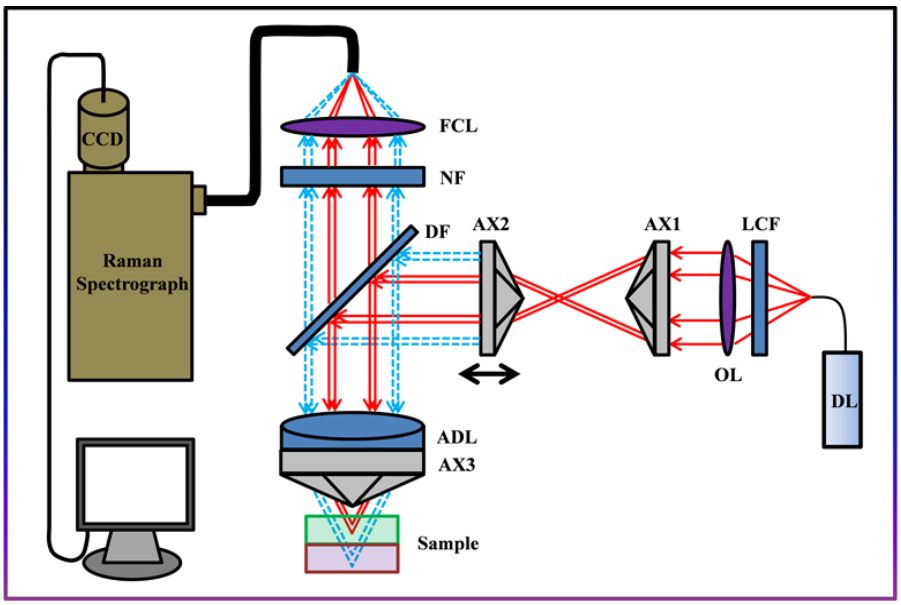

Fig 48: Experimental setup for the cone-shell Raman spectroscopy system

9. Raman optical tweezers for cell cycle analysis

The potential of Raman optical tweezers for label free cell cycle analysis has been demonstrated on human colon adenocarcinoma (Colo-205) cells in different phases of the cell cycle. It was shown that the DNA Raman band at 783 cm^{-1} can provide information about the DNA content (Fig. 49). The underlying motivation was to take the advantage of label free analysis of cells flowing in a suspension while remaining functionally active even after the analysis. The Raman spectra of optically trapped Colo-205 cells synchronized in G0/G1 and G2/M phases showed that the DNA Raman band at 783 cm-1 in the Raman spectra of optically trapped cells could provide information about the DNA content in the nucleus of the cells without the need for isolation of nucleus and therefore, could be considered as a label-free indicator of the DNA content. The results of these studies showed the utility of Raman optical tweezers for label free cell cycle analysis.

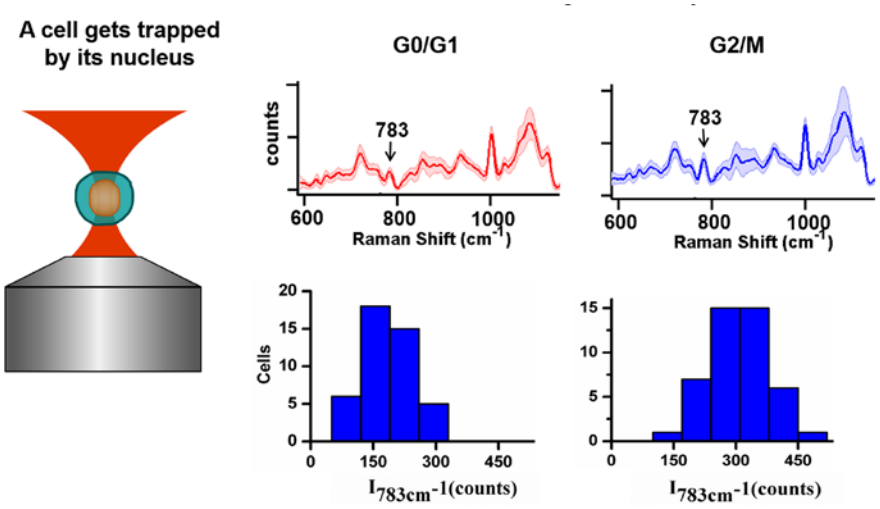

Fig 49: Raman spectra of optically trapped cells in different stages of cell cycle

10. Laser additive manufacturing of nuclear components

A laser additive manufacturing (LAM) system comprising of a 2 kW fiber laser, twin powder feeder and a 5-axes CNC workstation (Fig. 50) has been used for fabrication of nuclear components not possible to manufacture by conventional methods. In prototype fast breeder reactor (PFBR), regulating the flow distribution of liquid sodium as per the power level is required to remove fission heat. Honey-comb geometry orifice is one such permanent pressure dropping device used in the foot of the PFBR core sub-assembly. It has a complex structure with several hubs and ribs joining each other. Orifices fabricated with conventional precision fabrication methods have yielded a limited success and better dimensional control and surface finish is desired. Hence, LAM of these orifices was taken up. Fig.51 shows the fabricated structure. After metrological evaluation, the orifices have been provided to Indira Gandhi Centre for Atomic Research (IGCAR) for further tests.

Fig. 50: Laser additive manufacturing (LAM) in process.

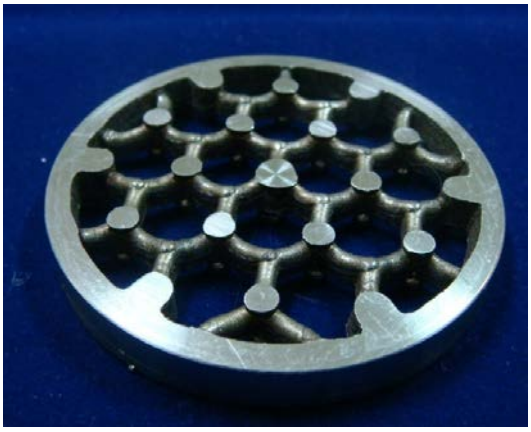

Fig. 51: A stainless steel orifice plate for the fast breeder reactor fabricated by LAM.

11. Prototype nuclear fuel pellet inspection system

A prototype machine vision based computerized inspection system has been designed and developed (Fig. 52) for quality assurance of the fuel pellets used in pressurized heavy water reactors (PHWR). It can inspect cylindrical surface of eight pellets in three seconds and each end face in 400 msec. The system is able to detect and categorize various surface defects like pits, chips and cracks (Fig. 53). This setup was qualified at Nuclear Fuel Complex for characterization of various surface defects. NFC is developing the pellet handling mechanism.

Fig. 52 : The line camera system for fuel pellet inspection.

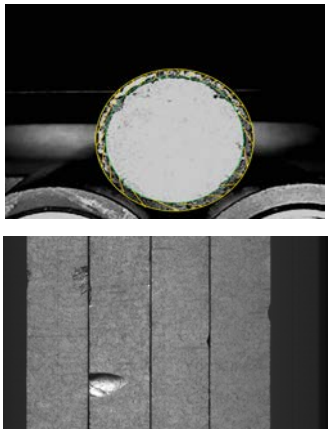

Fig. 53 : Images of fuel pellets with chip defects.
Top : Cylindrical surface of four pellets.
Bottom : End cap image of one pellet.

12. Development of fiber Bragg grating (FBG) based distributed temperature sensor

An in-house developed copper vapour laser based fiber Bragg grating (FBG) inscription setup (Fig. 54) has been used to fabricate distributed temperature sensor with four FBGs in a single fiber for temperature measurement upto 500 ^{0}C.

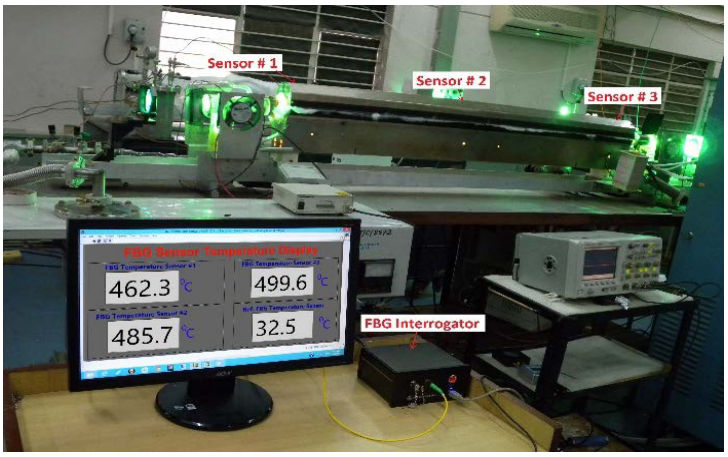

Fig 54: Fiber Bragg grating setup

13. Two-color femtosecond optical Kerr gate

A two-color femtosecond optical Kerr gate setup has been developed (Fig. 55) which can be used for sub-picosecond measurement of non-degenerate Kerr nonlinearity as well as transient photoluminescence of materials for ultrafast opto-electronic devices. The nonlinear material is gated by a ~100 femtosecond laser pump pulse and probed by its second harmonic. This technique allows

measurement of the magnitude, rise time as well as decay time of the Kerr nonlinearity of the material over a range of wavelengths allowed by the laser tunability (690-1040 nm in the present case). With CS_2 as the nonlinear material, a gating time as short as 350 fs has been obtained (Fig. 56).

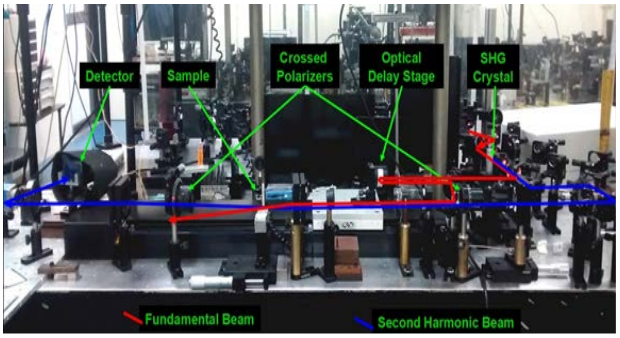

Fig. 55: Femtosecond two-color Kerr gate setup

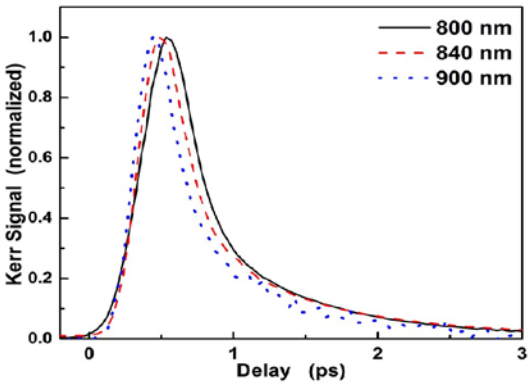

Fig.56 : The Kerr signal from CS_2 at different pump wavelengths showing a reduction in gate width with increasing wavelength.

14. Development of a laser based silica fiber drawing system and a laser based system for micro-machining of metals

A fiber drawing system has been designed and developed (Fig. 57) for drawing fused silica fibers suitable as suspensions to isolate optical components of a high-resolution displacement interferometer from ground noise. The system makes use of a 50W sealed CO2 laser and a pair of diamond turned axicon optics to symmetrically heat a 3mm “pre-form” fused silica rod and a servo driven pulling mechanism to draw the pre-form rod into a 600 microns diameter fiber. A servo control system was also developed to simultaneously control the laser power, the pre-form in-feed rate and the pulling rate to maintain the specified diameter. Testing and trials of the integrated system has been completed. A fiber laser based system has been designed and developed (Fig. 58) to micro-machine_metals. The developed system has a micro-machining area of 100mm diameter with a minimum feature size of 50 microns. The system was developed as per requirements of the Precision Engineering Division, BARC for micro-machining of features in metals and micro-structuring of metal foils.

Fig. 57: The laser based fiber drawing system

Fig. 58: The photo of the developed fiber laser micro-machining system.

15. Development of a toroidal trap for laser-cooled ^{87}Rb atoms by RF dressing of a quadrupole trap

The trapping of laser-cooled ^{87}Rb atoms in a toroidal geometry has been demonstrated using a RF-dressed quadrupole magnetic trap formed by superposing a strong radio frequency (RF) field on a quadrupole trap. This RF-dressed quadrupole trap has minimum of the potential away from the quadrupole trap centre on a circular path which facilitates the trapping in the toroidal geometry. Cold atom trapping in toroidal geometry has applications in the study of coherence, super-fluidity, Josephson oscillations, realization of atom gyroscope etc. The experiments were performed using a double magneto-optical trap (MOT) setup. The cold atoms in the second MOT were loaded in the RF-dressed toroidal trap by applying a RF field of appropriate frequency and power. The number of atoms trapped in the toroidal trap was typically ~1.3×10^5 with a temperature of ~40 μK.

V. MATERIALS SCIENCE

1. Growth and characterization of crystals for laser and related applications

Several high-quality crystals have been grown by different techniques for various photonic applications. These include Er and Cr co-doped YVO_4 for lasers, Cr-doped $Sr_{0.61}Ba_{0.39}Nb_2O_6$ (SBN) crystals for pyroelectric infrared sensors, and trans-stilbene for scintillation detectors (Fig. 59). Er^{3+} doped Yttrium ortho-vanadate YVO_4 generates two important laser emissions at ~1.55 and 2.9 μm, useful for high speed optical communication and gas sensing applications, respectively. Co-doping with Yb help in creating efficient population inversion in the upper state of Er ion. Yb-Cr co-doped YVO_4 has a potential use as self Q-switched laser gain medium. Strontium barium niobate (SBN) crystals were grown with different dopants to optimize their pyroelectric properties. A pyroelectric infrared sensor was fabricated from the grown SBN crystal and tested for the detection of 1064 nm, 7ns Nd:YAG laser pulses. Trans-stilbene (tSB) is useful organic scintillator material, particularly for detection of fast neutrons in the presence of gamma radiation background from radioactive materials. Platelets of tSB crystals were grown by low temperature solution growth with a new solvent, acetone.

Fig. 59: Photographs of some high optical quality crystals grown using different techniques. (a) Cr co-doped YVO_4, (b) $Sr_{0.61}Ba_{0.39}Nb_2O_6$ (SBN), (c) trans-stilbene.

2. Technology development for producing niobium-316L stainless steel brazed transition joints for superconducting RF cavities and copper-316L stainless steel brazed transition joints made without electroplating

Development of reliable Nb-316L stainless steel (SS) transition joints is an important step towards use of austenitic SS helium vessel for superconducting radio frequency (SCRF) cavities of particle accelerators. A new indigenous process has been developed to produce Nb pipe/316L stainless steel flange joints (Fig. 60) suitable for use in low-beta SCRF cavities. The highlights of the new process are (i) freedom from brittle intermetallics, (ii) uniform and controlled braze gap, (iii) efficient utilization of braze filler metal, (iii) simplified pre-braze fitting procedure and (iv) environment friendly cleaning procedure and (v) simple storage conditions for pre-braze assembly.

OFE copper-316L stainless steel (SS) transition joints find extensive application in particle accelerators all over the world. The usual practice for vacuum brazing of this transition joint

involves electroplating SS part with Ni or Cu. In this context, defect-free brazed Cu-316L SS transition joints have been prepared without recourse to electroplating (Fig. 61). Such transition joints find widespread applications in many particle accelerators components such as radio-frequency cavities of linear accelerators, radiofrequency quadrupoles, vacuum chambers for high brilliance machines, photon absorbers, profile transition chambers for insertion devices, pinhole assemblies etc.

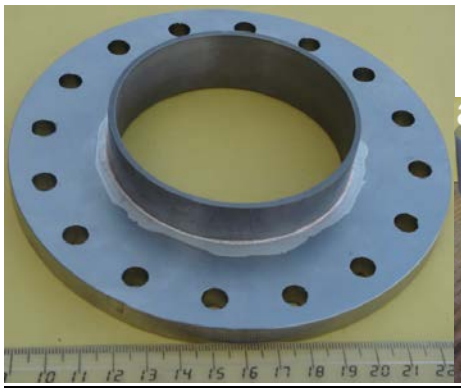

Fig. 60 : Nd pipe and stainless steel flange joint

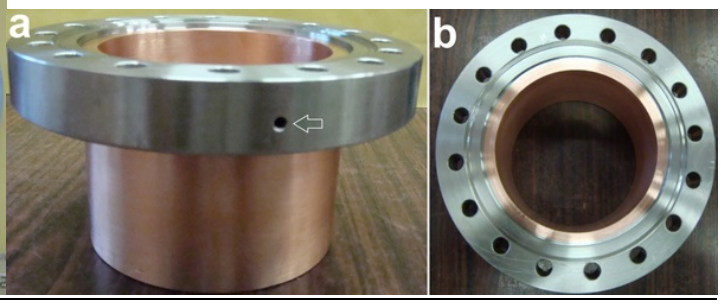

Fig. 61: (a) Side and (b) top views of vacuum brazed port joint between OFE copper and unplated 316L SS.

3. Investigations on magnetic, electron transport, thermal, electrical and mechanical properties of materials of potential technological applications

Basic research on various properties of materials of technological interest is being conducted using the synchrotron radiation source, lasers and other sophisticated laboratory facilities developed at RRCAT. These include investigation of saturation magnetization of Gd doped lead magnesium niobate (PMN), structural phase transition studies on barium-calciumTiO_3 ferroelectric ceramic by micro-Raman scattering, demonstration of electric field controlled reproducible non-volatile uni-polar resistive memory switching in amorphous gold/TiO_2/platinum device structures, observation of weak localization in 2-dimensional electrons gas confined at polar semiconductor heterostructures, observation of phase-coherent electron transport in (Zn, Al)O_x thin films grown by atomic layer deposition**,** observation of structural phase transition of ternary high (k~ 22) gate dielectric $SmGdO_3$ using high pressure angle dispersive x-ray diffraction for memory applications, synthesis of Mo-Re superconductor alloys and study of their magnetic and thermal properties.

Knowledge of mechanical properties is important for assessing the technological applicability of superconductors. An experimental facility (Fig. 62) based on the resonant ultrasound spectroscopy technique was designed and developed for the measurement of the elastic constants of such materials as functions of temperature (2 to 300 K) and magnetic field (up to 70 kOe). It is being used to study the mechanical properties of Mo-Re alloys, which are alternative materials to niobium in accelerator technology.

Fig. 62: Experimental facility of Resonant Ultrasound Spectroscopy for the measurement of the elastic constants materials at low temperatures (2-300 K) and in high magnetic fields (up to 70 kOe).

VI. INTERNATIONAL COLLABORATION

1. Development of 20 kW, 499.75 MHz, pulsed solid state power amplifier under DAE-CERN collaboration

A 20 kW pulsed solid state amplifier and its 5 kW prototype amplifier system were designed and developed for the CLIC facility at CERN, Geneva (Fig. 63). The prototype amplifier was first shipped to CERN for performance evaluation after which the fabrication of the 20 kW amplifier was completed. The 20 kW amplifier was thoroughly tested for its performance inclusive of heat runs of over 200 hrs. The amplifier has now been shipped to CERN.

2. Development of 30kW, 650 MHz solid state RF amplifier under Indian Institutions-Fermilab Collaboration

A 30 kW solid state amplifier at 650 MHz has been designed and developed (Fig. 64) for the international collaboration program under Indian Institutions-Fermilab Collaboration (IIFC). In this design, 15 kW of RF power was obtained by summing power output of 40 numbers of 500 watts RF amplifier modules using 40-way power dividers and combiners and high power directional couplers. The output power of two such 15 kW RF amplifier racks was combined using 2-way power combiner to get 30 kW RF power. RF power of 30 kW was tested with 50 ohms standard water cooled RF dummy load.

Fig. 63: The 20 kW, 499.75 MHz solid state amplifier developed for the CERN CLIC facility.

Fig. 64: The 30 kW, 650 MHz solid state amplifier developed under the Indian Institutions- Fermilab Collaboration.

VII. INFRASTRUCTURE

1. Computing infrastructure

The aggregate computing power available to scientists and engineers in RRCAT now stands at 43.08 Teraflops with integration of a high performance computing cluster, Kshitij-4. Software for RRCAT Secure Cloud Drive (Fig. 65) has been developed, deployed and released to senior scientists. The facility enables access to large files over internet with necessary data security mechanisms in place. Workflow based software for activity management related to Indus up-gradation / maintenance/ shutdown has been developed and deployed on RRCAT Infonet for use by all concerned officials working for Indus operation and maintenance. Web based MIMIC panel for electric fence was developed and deployed for identifying location of the fault on a graphical representation.

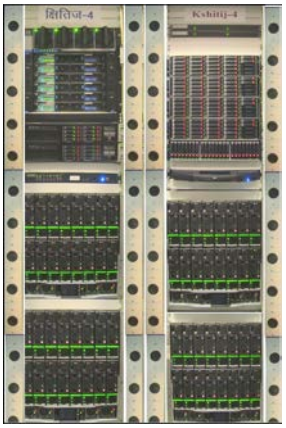

Fig. 65. Schematic diagram of RRCAT secure cloud drive.

2. Civil infrastructure

Construction and electrification of Petawatt laser laboratory building (Fig. 66), Infrared free electron laser user's laboratory building (Fig. 67), Cavity processing laboratory building, Diamond Jubilee Guest house (Fig. 68), Diamond Jubilee Park (Fig. 69), and 12 nos. type V-E houses have been completed. A new substation has been set up in North side area of RRCAT to take care of power requirements of upcoming labs. Micro-irrigation (drip) system has been installed for the gardens in the laboratory area.

Fig. 66 : Petawatt laser laboratory building.

Fig. 67: Infrared free electron laser user's laboratory building.

Fig. 68: Diamond Jubilee Guest house

Fig. 69: Diamond Jubilee Park at dusk with Sukhniwas lake in the background

VIII. HUMAN RESOURCE DEVELOPMENT

Human resource development activities at RRCAT have been greatly enhanced by extending the available research facilities for training of university students in the areas of accelerators, lasers and their applications. A large number of students are carrying out research work at RRCAT for their PhD degree under the framework of Homi Bhabha National Institute. Opportunities are also provided to M.Tech. / M.Sc. students (Fig. 70) to carry out their one-year / six-months project work towards partial fulfillment of their degrees.

Fig. 70: M.Tech / M.Sc students working on project works related to lasers, Indus accelerators and beamlines utilization.

IX. OUTREACH ACTIVITIES

The first Orientation Course on Accelerators, Lasers and related Science and Technologies (OCAL-2015) started this summer was attended by 40 students selected from all over the country (Fig. 71). All students completed the course successfully and were awarded certificates by Dr. M.R. Srinivasan, Member AEC and Former Chairman, AEC & Secretary, DAE.

Under the Public Outreach Programme, several events named “Kan aur Prakash Vigyan Saptah” were organized as part of Diamond Jubilee celebrations. These were held in various schools and colleges in Indore and in nearby cities and towns like Ujjain, Mhow, Dewas and Khargone. The events included an exhibition of specially developed working models (Fig. 72), posters describing the DAE programs and R&D activities of RRCAT, lectures and interaction sessions with RRCAT

scientists (Fig. 73). Concurrently, painting, essay and quiz competitions were also held. About 1500 to 2000 students and teachers faculty members participated in each event leading to a total participation over 12000 participants in various events.

Fig. 71: OCAL-2015 students with some of the faculty.

Fig 72: Students being shown a working model of Indus-2.

Fig. 73: A public outreach event in a school.